Electronic Supplementary Material (ESI) for Environmental Science: Nano.

Supplementary Information for

Residence Lifetimes of Nanoconfined CO_2 in Layered Aluminosilicates

Merve Yeşilbaş*, Michael Holmboe, and Jean-François Boily*

Department of Chemistry, Umeå University, SE-901 87 Umeå, Sweden

- co-corresponding authors: merve.yesilbas@umu.se; jean-francois.boily@umu.se

This Supplementary Information file includes:

Table of Content

1. Evaluation of initial quantities of water in MMT

Interlayer water was first evacuated by exposing MMT to a vacuum (<0.3 Pa, the detection limit of the capacitance manometer (MKS, Baratron)) for 30 min at 25 °C. This evacuation time was chosen after preliminary efforts revealed that it was sufficient to remove the great majority of water. This assessment was made by monitoring the bending region of water (Fig. S1), that however also showed a persistent population of water after this evacuation time and, as shown in Fig. S1, up to at least 40 min. Using the approach to be described in this section, we estimate that the water populations in the MMT samples prior, during and ensuing CO_2 intercalation and removal in vacuum (Fig. S2) are nearly constant and in the range 10-15 mg H_2O/g (0.6-0.8 mmole/g) (Eq.1) to 17-26 mg H_2O/g (0.9-1.4 mmole/g) (Eq. 2).

These results were obtained from a quantitative treatment of the response of the of 1630 cm^{-1} ν_3 band of water of the water vapour adsorption isotherm data of Yeşilbaş *et al.*[1]. This was achieved by linking FTIR data (Fig. S3 a) and microgravimetric data (Fig. S2 b) through the functions shown in Fig. S2 b. We used the band intensity (I) ratios of the 1630 cm^{-1} band of water and of the 1850 cm^{-1} band of MMT (combination of Si-O stretching and OH deformations, *e.g.* $\nu_{Si\text{-}O}$ (1003 cm^{-1}) +δ_{AlMgOH} (846 cm^{-1})). See caption of Fig. S3 for more details on the choice of this approach. We relate the microgravimetrically-derived changes in water mass (Δw) to changes in the band intensity ratios (I_{1630}/I_{1850}) through:

$$\Delta w = 0.0575\ (I_{1630}/I_{1850})^2 + 1.99\ (I_{1630}/I_{1850}) + 21.4 \qquad (1)$$

for a quadratic function, or alternatively through:

$$\Delta w = 4.065\ (I_{1630}/I_{1850}) + 36.4 \qquad (2)$$

for a linear function. Residual water levels in the N_2(g)-dried sample of Yeşilbaş *et al.*[1] are then estimated as -Δw at the intercept (I_{1630}/I_{1850}=0) of the function. (Fig. S3 b) We present both functional to show the sensitivity of the choice of the function on the estimation of initial water content at I_{1630}/I_{1850}=0. Thus, using Eq. 1 we obtain an initial water loading of 21.4 mg H_2O/g (1.2 mmole/g) or 36.4 mg H_2O/g (2.0 mmole/g) with Eq. 2 on MMT that was initially dried in N_2(g) for the Yeşilbaş *et al.*[1] study (*cf.* Fig. S4).

These water loadings would correspond to *d*-spacings of d_{001}=10.1 Å (Eq. 1) to d_{001}=10.5 Å (Eq. 1) if we apply the following equation[2]:

$$d_{001} = \frac{2}{s_A \rho_w} \times \frac{g_{H_2O}}{g_{clay}} + t_{MMT} \qquad (3)$$

where the specific surface area (s_A) is 750 m^2/g, the interlayer water density (ρ_w) is 1 g/cm^3, and the thickness of dry MMT layers (t_{MMT}) is approx. 9.5 Å. They consequently support the concept that the interlayer region of N_2(g)-dried MMT are still partially expanded, and thus capable of accommodating CO_2.

In an effort to validate those results, we measured the *d*-spacing of MMT samples which was dried with N_2(g) for 12 h using X-ray diffraction (XRD). Mixed layer modelling of the XRD data of Fig. S5 (*cf.* Section 2 for details on modelling), give an average d_{001}=10.19 Å from an interlayer composed of 74 % 0W, 18 % 0.5W and 8% 1W. Using Eq. 3, this value can also be used to a residual water content of 25.9 mg H_2O/g MMT (1.4 mmole/g). This water content falls between our above-mentioned range of values of 21.4 -36.4 mg H_2O/g from Eqs. 1 and 2. We also show that heating the MMT sample to 105 °C for 2 h under a stream of N_2(g) decreases the *d*-spacing down to 9.87 Å (87 % OW, 13 % 1W), and therefore that even longer periods are needed to completely dehydrate MMT.

2. Evaluation of water under sub-freezing conditions

Eqns. 1 & 2 could not be used to estimate intercalated water loadings under subfreezing conditions, the presence of ice outside the particles, manifested through a broader and less intense bending band. As a result, another calibration curve based on the intensity ratios of the 3393 (water O-H) and 3628 (bulk OH + water O-H; *cf.* Yeşilbaş *et al.*[1]) bands was preferred (Fig. S8). The 3393 cm^{-1} was chosen given the low absorbances of ice at this wavenumber.

3. X-ray diffraction and mixed layer modelling

The MMT interlayer expansion was determined by X-ray diffraction (XRD) using an PANalytical X'Pert[3] Powder diffractometer equipped with a MHC-trans non-ambient chamber working in transmission mode at 45kV and 40mA. XRD profiles were collected in the 2-50° (2θ) range using CuK_α radiation at a resolution of 0.0334° per step on (1) one sample dried to 105 °C for 2 h under a flow of N_2(g), then cooled to 25 °C, and (2) a sample degassed at 25 °C with N_2(g) over a 12 h period. All data was background corrected for the chamber housing and difference in path length due to the transmission geometry.

The XRD profiles *00l* reflections (upto the fifth order) and the average MMT basal spacing, was fitted simultaneously using one-dimensional mixed-layer modelling.[1-4] This was accomplished with an in-house code OneDXRD based on the recursive algorithm used in the Newmod software[3], allowing modelling of 2 or 3 interstratified custom structural components, a log normal MMT stack size distribution, size strain, and so-called mega-crystal correction.

The XRD profiles from the heated and N_2-dried samples were modelled with two and three components, respectively, consisting of two mixed subcomponents (MMT layers at different hydration states) having basal spacings of 9.6, 11.5 and in the case of the N_2-dried sample also 12.2 Å, respectively, corresponding to 0W, 0.5W and 1W hydration states. All structural parameters for the MMT lattice were taken from Moore and Reynolds[3] whereas all interlayer parameters were taken from molecular dynamics simulations from a previous study.[1]

FIGURES

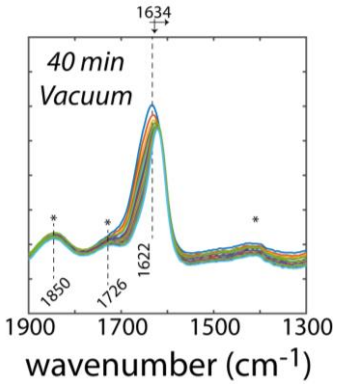

Figure S1. Water-bending region of Na-MMT under vacuum (< 0.3 Pa) for up to 40 min (n.b. Samples were dried *in vacuo* for 30 min for this work). Asterices (*) denote MMT bands unaffected by dehydration. The 1850 cm^{-1} band is used in Fig. S2 as an internal reference to predict water loadings in MMT. Experimental results taken from Yeşilbaş *et al.* [1].

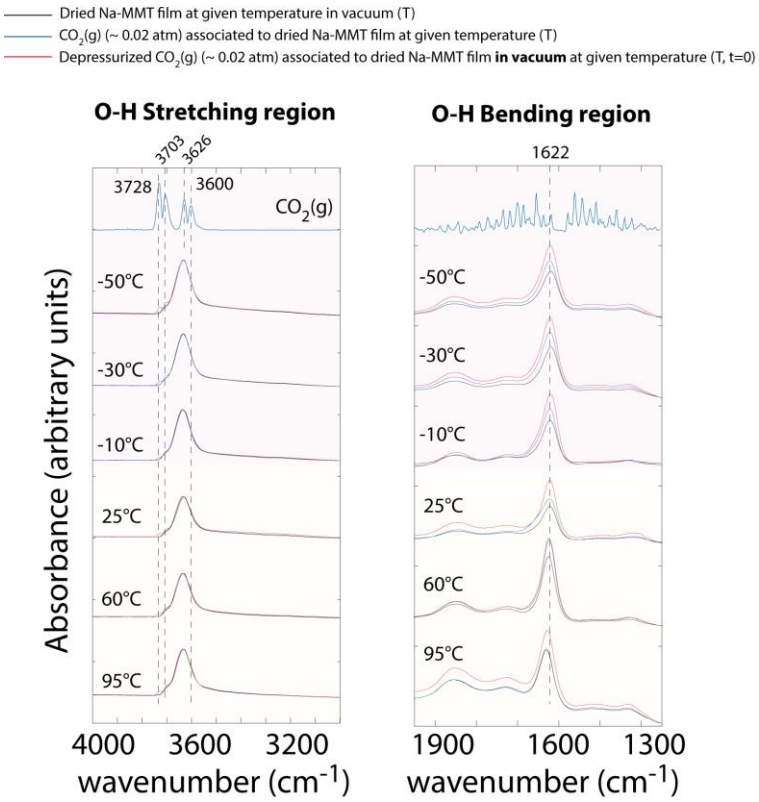

Figure S2. O-H stretching and water bending regions of MMT prior, during and ensuring intercalation of CO_2. The bending region shows a near constancy of water loadings during the experiments. The band intensity ratios between the 1630 cm^{-1} and the 1850 cm^{-1} bands suggest water loadings of 10-15 mg H_2O/g MMT (*cf.* Fig. 2). To this dataset we include additional data at 95 °C to demonstrate further the persistency of the interlayer water.

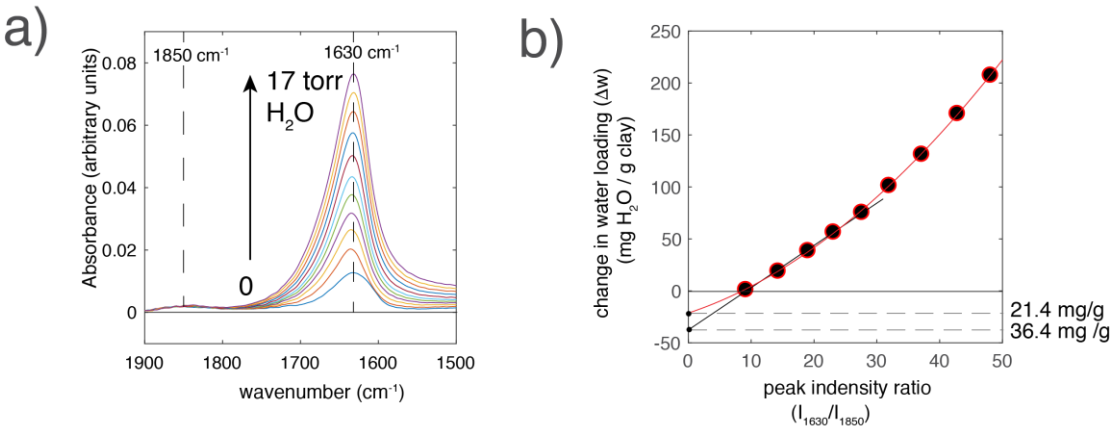

Figure S3. Numerical evaluation of intercalated water content in Na-MMT based on the band intensity ratios of the 1630 cm^{-1} ν_3 band of water and the 1850 cm^{-1} band resulting from combination modes of the Si-O stretching and OH deformation region of MMT (*e.g.* $\nu_{Si\text{-}O}$ (1003 cm^{-1}) $+\delta_{AlMgOH}$ (846 cm^{-1})) (a). The calibration (b) was built using the experimental data water vapour binding data of Yeşilbaş *et al.*[1], combining (a) FTIR and microgravimetric data. It was then shifted to w = 0 at $I_{1630}/I_{1850} = 0$. The offset was of 21.4 mg H_2O/g MMT (Eq. 1) to 36.3 mg H_2O/g MMT (Eq. 2), which is the residual amount of water in MMT after degassing with dry N_2(g). The calibration curve can be calculated with the Matlab code given in Table S6. Other calibration curves could be built with the bulk OH stretch (3630 cm^{-1}) or the Si-O stretch (1003 cm^{-1}), however not without posing uncertainties with respect to sloping baselines for distal bands, or the limitations in measuring bands < 1200 cm^{-1} in our optical cells equipped with CaF_2(s) windows. The vicinity and water pressure independence of the 1850 cm^{-1} band represents an ideal reference for MMT.

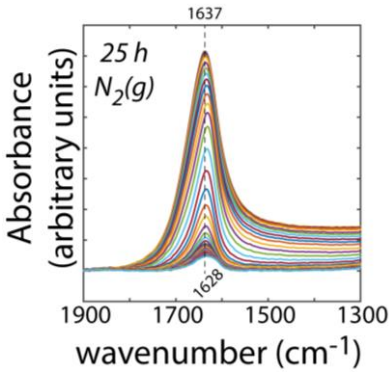

Figure S4. Water-bending region of Na-MMT under drying with N_2(g) for 25 h on ATR diamond cell. Experimental results taken from Yeşilbaş *et al.*[1].

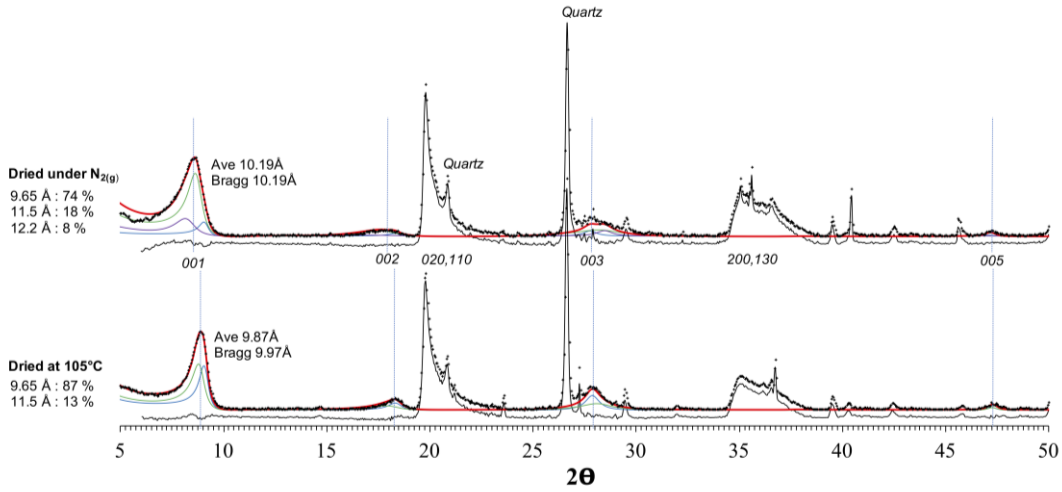

Figure S5. XRD profiles for the Swy-2 MMT samples dried either by heating (bottom) at 105°C for 2 h, or with dry N_2-gas (top) for 12 h. Accessory minerals were not removed in these samples, and were not accounted for in XRD modelling. The non-rational *00l* reflections of MMT were fitted with 2 and 3 interstratified components, each consisting of two (phase A and phase B) randomly interstratified subcomponents, corresponding to the 9.65 Å (phase A) and the 11.5 or 12.Å (phase B) hydration states. The total fraction (in percent) of each basal spacing/hydration states is indicated to the left. The average basal spacing obtained by drying with N_2-gas was found to be approx. 0.3 Å, or ~1/10 of a water layer, larger than when dried under heating. The increased degree of hydration state heterogeneity was also evident from the so-called irrationality parameter indicating non-rational reflections, which was 0.15 and 0.33 for the heated and N_2-dried sample, respectively.

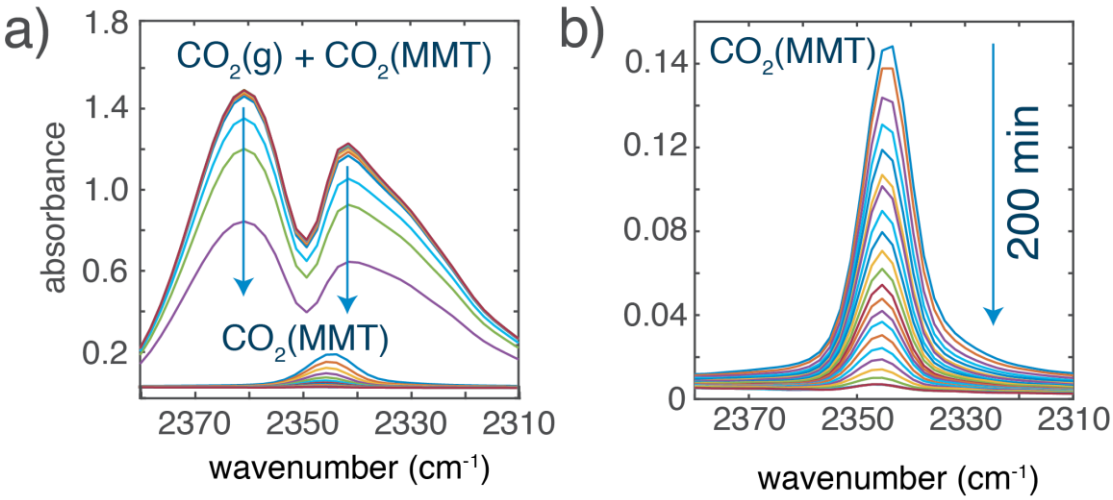

Figure S6. Asymmetric (ν_3) stretching region of CO_2 of MMT (~0W) originally exposed to CO_2(g) at -30°C. (a) Free and MMT-intercalated CO_2 and (b) only MMT-intercalated CO_2 during 200 min of evacuation (< 0.3 Pa) at -30°C.

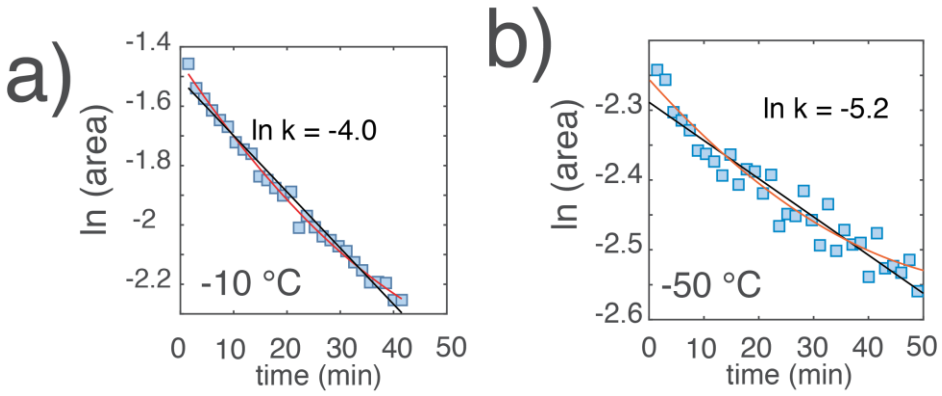

Figure S7. Instantaneous CO_2 removal rates (red lines) were obtained by the first derivative of a 2nd order polynomial function of ln (area) *vs. t* of data, as shows in the red lines of (a) and (b). This is an example of how values were obtained for Fig. 4 of main text.

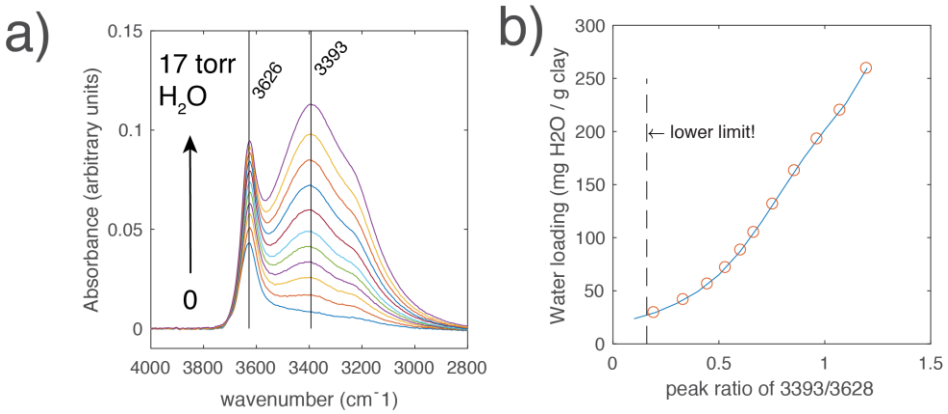

Figure S8. Numerical evaluation of high values of intercalated water content in Na-MMT, based on the band intensity ratios 3393 cm^{-1}/3628 cm^{-1}. Calibration was built using the experimental data of Yeşilbaş *et al.*[1], combining FTIR and microgravimetric data. This curve was used to estimate water content in MMT at -10°C and -50°C because the calibration curve based on the water bending mode (Fig. S3) is altered by the formation of ice.

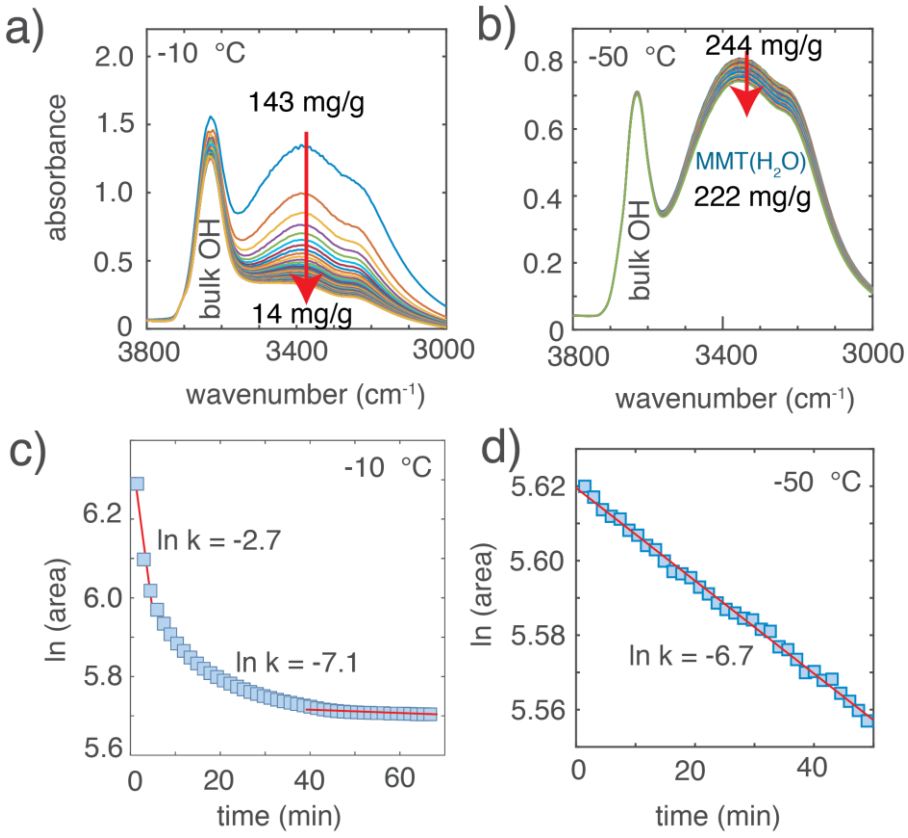

Figure S9. (a-b) O-H stretching region showing bulk MMT hydroxyl (bulk OH) and interlayer (MMT(H_2O)) content during evacuation of CO_2-loaded MMT at (a) -10 °C and (b) -50 °C. (c) and /(d) show rates of water removal, estimated by the area of the 3000-3550 cm^{-1} region.

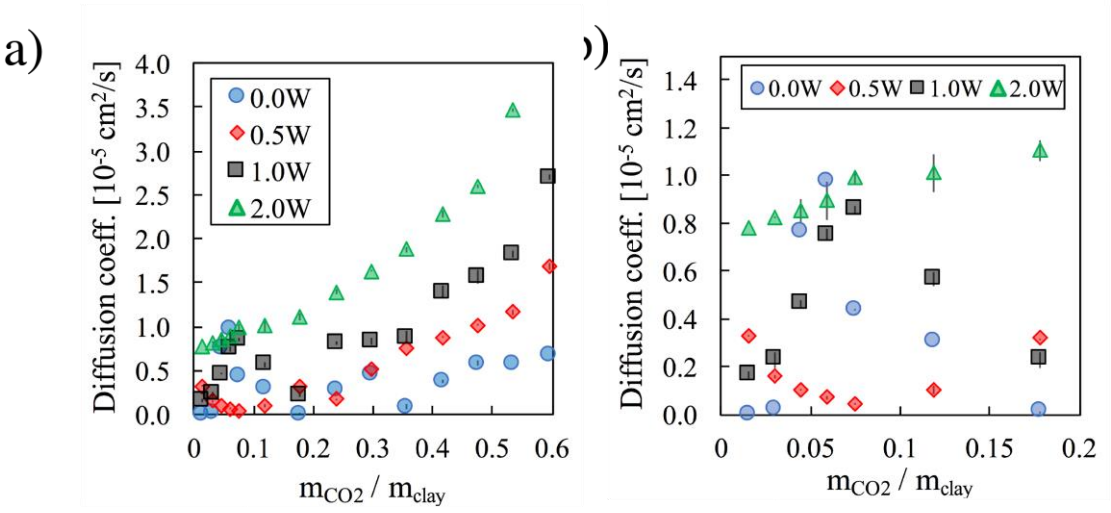

Figure S10. Computed diffusion coefficients of CO_2 in the interlayer region of MMT (298 K). (a) all CO_2 loadings considered in this work. (b) The lower range of CO_2 loadings (< 0.2 gCO_2/g MMT).

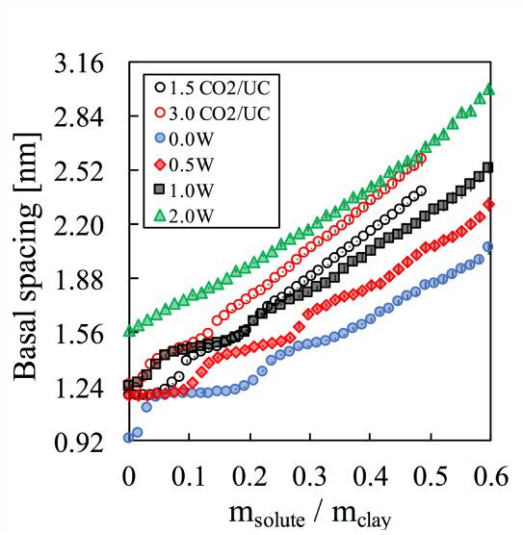

Figure S11. Basal spacing (d_{001}) obtained from the layer-to-layer distance in the MD simulations at fixed CO_2 (open symbols) and fixed water loadings (filled symbols). These data show a non-linear and step-wise dependence upon different loadings of CO_2 and water molecules, in parallel behavior to hydrated MMT without intercalated CO_2.[5] This indicates a preference for discrete 1- and 2-layered states regardless of the CO_2/H_2O ratio.

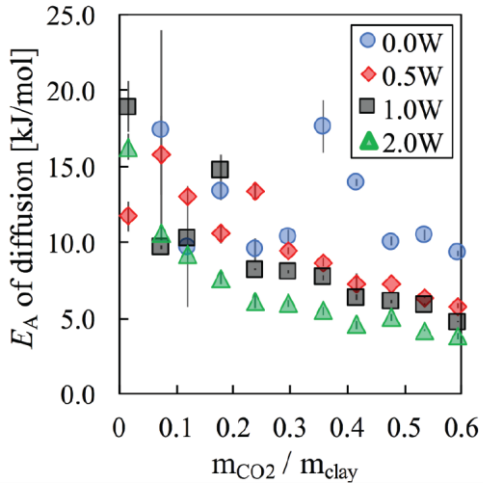

Figure S12. Computed Activation energies (E_a) for CO_2 diffusion. Values were obtained from the Arrhenius relationship of diffusion coefficients obtained by Molecular Dynamics simulations from -10 to 50 °C. More erratic values of 0W result from limitations in sampling CO_2 of small diffusivity.

SUPPLEMENTARY TABLES

Table S1. Activation energies (E_a) of diffusion for interlayer CO_2 at different CO_2 and fixed water loadings (0.0W, 0.5W, 1.0W and 2.0W). The activation energies were calculated from the linearized Arrhenius equation and four diffusion coefficients, at 263, 283, 298 and 323K.

m_{CO2}/m_{clay}	***0.015***	***0.074***	***0.119***	***0.178***	***0.238***	***0.297***	***0.357***	***0.416***	***0.476***	***0.535***	***0.595***
0.0W	-	17.45	9.70	13.38	9.51	10.32	17.57	13.91	10.05	10.49	9.28
	-	±6.53	±3.98	±0.59	±0.71	±0.45	±1.73	±0.21	±0.29	±0.36	±0.13
0.5W	11.70	15.73	12.97	10.54	13.32	9.47	8.67	7.28	7.24	6.37	5.80
	±1.02	±2.59	±0.19	±0.60	±0.58	±0.26	±0.29	±0.61	±0.01	±0.09	±0.14
1.0W	18.93	9.65	10.25	14.73	8.22	8.07	7.70	6.34	6.15	5.91	4.77
	±1.70	±0.14	±0.16	±1.00	±0.05	±0.10	±0.19	±0.17	±0.12	±0.06	±0.06
2.0W	16.30	10.56	9.19	7.65	6.14	6.01	5.52	4.55	5.05	4.18	3.80
	±0.90	±0.44	±0.32	±0.39	±0.51	±0.27	±0.28	±0.27	±0.20	±0.08	±0.23

Table S2. Diffusion coefficients for CO_2 in the **0.0W** MMT interlayers (in cm^2/s) at different temperatures and CO_2 loadings, also indicated by the corresponding different d_{001}.

m_{CO2}/m_{clay}	***0.015***	***0.074***	***0.119***	***0.178***	***0.238***	***0.297***	***0.357***	***0.416***	***0.476***	***0.535***	***0.595***
d_{001}[Å]	***0.97***	***1.20***	***1.21***	***1.23***	***1.39***	***1.49***	***1.55***	***1.68***	***1.80***	***1.91***	***2.06***
263 K	<0.001	0.322	0.231	0.004	0.162	0.250	0.040	0.182	0.328	0.327	0.406
	-	±0.001	±0.004	±0.003	±0.001	±0.017	±0.032	±0.007	±0.025	±0.003	±0.001
283 K	<0.001	0.387	0.388	0.006	0.207	0.366	0.059	0.280	0.457	0.443	0.544
	-	±0.002	±0.007	±0.005	±0.001	±0.015	±0.018	±0.001	±0.016	±0.012	±0.001
298 K	<0.001	0.437	0.301	0.008	0.275	0.450	0.089	0.386	0.579	0.577	0.674
	-	±0.002	±0.000	±0.003	±0.001	±0.018	±0.038	±0.020	±0.026	±0.002	±0.001
323 K	<0.001	1.522	0.593	0.012	0.356	0.603	0.175	0.591	0.766	0.790	0.890
	-	±0.002	±0.004	±0.002	±0.002	±0.005	±0.016	±0.065	±0.051	±0.012	±0.001

Table S3. Diffusion coefficients for CO_2 in the **0.5W** MMT interlayers (in cm^2/s) at different temperatures and CO_2 loadings, also indicated by the corresponding different d_{001}.

m_{CO2}/m_{clay}	***0.015***	***0.074***	***0.119***	***0.178***	***0.238***	***0.297***	***0.357***	***0.416***	***0.476***	***0.535***	***0.595***
d_{001}[Å]	***1.19***	***1.22***	***1.33***	***1.45***	***1.50***	***1.67***	***1.77***	***1.85***	***2.02***	***2.13***	***2.32***
263 K	0.160	0.019	0.049	0.189	0.079	0.314	0.472	0.564	0.691	0.826	1.238
	±0.001	±0.015	±0.009	±0.005	±0.009	±0.006	±0.003	±0.006	±0.014	±0.018	±0.024
283 K	0.231	0.024	0.074	0.264	0.129	0.435	0.645	0.754	0.872	1.004	1.469
	±0.020	±0.002	±0.009	±0.006	±0.012	±0.008	±0.005	±0.009	±0.008	±0.022	±0.032
298 K	0.327	0.043	0.099	0.315	0.169	0.517	0.757	0.879	1.018	1.161	1.683
	±0.002	±0.005	±0.018	±0.006	±0.007	±0.007	±0.006	±0.007	±0.014	±0.035	±0.043
323 K	0.420	0.067	0.146	0.469	0.247	0.708	0.992	1.047	1.277	1.417	2.020

	±0.005	±0.006	±0.011	±0.005	±0.013	±0.010	±0.005	±0.005	±0.019	±0.025	±0.072

Table S4. Diffusion coefficients for CO_2 in the **1.0W** MMT interlayers (in cm^2/s) at different temperatures and CO_2 loadings, also indicated by the corresponding different d_{001}.

m_{CO2}/m_{clay}	***0.015***	***0.074***	***0.119***	***0.178***	***0.238***	***0.297***	***0.357***	***0.416***	***0.476***	***0.535***	***0.595***
d_{001}[Å]	***1.26***	***1.44***	***1.48***	***1.53***	***1.70***	***1.80***	***1.94***	***2.08***	***2.20***	***2.35***	***2.54***
263 K	0.052	0.504	0.322	0.094	0.522	0.543	0.580	1.010	1.116	1.338	2.102
	±0.011	±0.021	±0.013	±0.037	±0.006	±0.030	±0.079	±0.058	±0.053	±0.012	±0.010
283 K	0.092	0.699	0.451	0.165	0.684	0.701	0.760	1.233	1.377	1.609	2.452
	±0.003	±0.024	±0.019	±0.033	±0.012	±0.039	±0.055	±0.092	±0.065	±0.020	±0.020
298 K	0.164	0.854	0.567	0.227	0.816	0.829	0.882	1.396	1.568	1.832	2.701
	±0.016	±0.017	±0.031	±0.031	±0.016	±0.035	±0.075	±0.073	±0.074	±0.040	±0.028
323 K	0.246	1.146	0.767	0.329	1.050	1.078	1.119	1.736	1.882	2.209	3.156
	±0.021	±0.030	±0.018	±0.028	±0.022	±0.026	±0.124	±0.095	±0.082	±0.035	±0.036

Table S5. Diffusion coefficients for CO_2 in the **2.0W** MMT interlayers (in cm^2/s) at different temperatures and CO_2 loadings, also indicated by the corresponding different d_{001}.

m_{CO2}/m_{clay}	***0.015***	***0.074***	***0.119***	***0.178***	***0.238***	***0.297***	***0.357***	***0.416***	***0.476***	***0.535***	***0.595***
d_{001}[Å]	***1.60***	***1.74***	***1.80***	***1.92***	***2.05***	***2.17***	***2.31***	***2.45***	***2.60***	***2.80***	***3.00***
263 K	0.307	0.584	0.598	0.753	1.054	1.212	1.417	1.822	2.015	2.760	3.846
	±0.038	±0.159	±0.153	±0.144	±0.131	±0.119	±0.161	±0.138	±0.100	±0.039	±0.027
283 K	0.576	0.818	0.807	0.983	1.257	1.442	1.641	2.057	2.372	3.188	4.370
	±0.082	±0.190	±0.187	±0.160	±0.140	±0.170	±0.178	±0.159	±0.128	±0.031	±0.054
298 K	0.775	0.989	1.010	1.106	1.394	1.633	1.878	2.277	2.595	3.464	4.631
	±0.055	±0.170	±0.198	±0.197	±0.180	±0.160	±0.201	±0.159	±0.105	±0.015	±0.056
323 K	1.242	1.446	1.297	1.458	1.790	2.022	2.256	2.680	3.109	3.943	5.345
	±0.015	±0.163	±0.153	±0.178	±0.159	±0.154	±0.119	±0.145	±0.034	±0.105	±0.035

Table S6. Matlab (The Mathworks, Inc). code for estimation of intercalated water loadings in Na-MMT at 298 K

```
function [water]=MMTwater(wavb,B5)

% This code estimates adsorbed water loading on Na-MMT from
% the intensity ratios of the bending band of
% intercalated water (1630 cm-1) and the combination/overtone of the
% Si-O and OH deformation of MMT bulk (1850 cm-1)
%
% water = mg H2O / g of clay
%
% Send questions/report problems to jean-francois.boily@umu.se

p=[0.0575    1.9967  0]; %parameters for 2nd order polynomial

z=size(B5);

if z(1) < z(2)
    B5=B5';
end

% sets Abs=0 at 1900 cm-1
i=find(round(wavb)==1900);
for n=1:size(B5,2)
    B55(:,n)=B5(:,n)-B5(i,n);
end
%

%calculate band intensity ratio
i=find(round(wavb)==1630);
ii=find(round(wavb)==1850);
peakra=B55(i,:)./B55(ii,:);

water=polyval(p,peakra);
%

%plot & print data and calibration curve
subplot(2,1,1);plot(wavb,B55,[1850 1850],[0 max(max(B5))],[1632 1632],[0
max(max(B5))]);
xlabel('wavenumber (cm^-1)');
ylabel('Absorbance (arbitrary units)');
subplot(2,1,2);plot(0:50,polyval(p,0:50),peakra,water,'o');
xlabel('peak ratio of 1630/1850');
ylabel('Water loading (mg H2O / g clay');

disp('in mg H2O per g clay')
```

References

1. M. Yeşilbaş, M. Holmboe and J.-F. Boily, *ACS Earth Space Chem.*, 2018, **2**, 38-47.
2. M. Holmboe, S. Wold and M. Jonsson, *J. Cont. Hydr.*, 2012, **128**, 19-32.
3. D. M. Moore and R. C. Reynolds, in *X-ray Diffraction and the Identification and Analysis of Clay Minerals*, Oxford University Press, Oxford, 1997, vol. 2nd Edition.
4. E. Ferrage, *Clays and Clay Minerals*, 2016, **64**, 348-373.
5. M. Holmboe and I. C. Bourg, *Journal of Physical Chemistry C*, 2014, **118**, 1001-1013.